Reduced Order Lumped Parameter Thermal Network for Dual Three-Phase Permanent Magnet Machines

P. Giangrande, V. Madonna, S. Nuzzo, C. Spagnolo, C. Gerada, M. Galea

***Abstract* – In recent years, electrical machines are employed in an ever-increasing number of safety-critical applications, which require high power density, along with a demanding level of reliability and/or fault-tolerance capability. Multi-phase machines are generally considered a suitable option for satisfying these constraints. Among them, the dual three-phase configuration claims the additional benefit of being operated through conventional power electronics converters and control strategies. Despite the undeniable advantages and their wide diffusion, the thermal modelling of dual three-phase machines still represents an open research topic. Thus, this paper proposes the thermal analysis of a dual three-phase permanent magnet synchronous machine, highlighting the thermal coupling between the two winding sets. An experimentally fine-tuned lumped parameter thermal network is initially presented. Then, due to its relatively high number of nodes, a reduced order thermal network using only 3 nodes is developed. Finally, both thermal networks are examined and compared under several load conditions, in terms of accuracy and computational burden.**

***Index Terms*—Dual three-phase, Fine-tuning, Multi-phase, LPTN, PMSM, Thermal management, Thermal modelling.**

I. Introduction

DUAL three-phase permanent magnet synchronous machines (PMSMs) are a viable design choice for safety-critical applications [1, 2]. Indeed, they can safely operate even in the event of severe failures, such as open- and short-circuit faults [3]. Compared with other topologies of multi-phase (i.e. number of phases higher than three) electrical machines (EMs), the dual three-phase winding arrangement allows to adopt standard three-phase power electronics converters (PECs) [4-6]. This is surely an advantage over e.g. five phase machines, where custom PECs and control strategies are required [7, 8].

When designing an EM, a complete and multi-physics approach should be considered by including electromagnetic, thermal, and mechanical aspects [9-11]. In fact, in modern applications, where high-performance needs to be reached in limited dimensional constraints, there is a drive towards boosted power density, i.e. achieving a compact design while increasing the power level [12]. Such tendency is leading to push the electromagnetic and thermal boundaries to the limit [13]. In this scenario, the thermal management plays a significant role [14, 15], as well as the thermal modelling [16, 17]. Indeed, over-temperatures, caused by either temporary overloads or winding faults, are to be avoided, since they might compromise the EM insulation lifetime [18, 19]. Therefore, thermal models are used for predicting the EMs' thermal behaviour and for identifying the hot-spots [20].

In literature, several works deal with the electromagnetic design of dual three-phase PMSMs and their performance in healthy and faulty operations [2, 4, 5, 21]. Further, a detailed thermal study is presented, in [4]. Nevertheless, it is not common to find a 'complete' lumped parameter thermal network (LPTN) for dual three-phase PMSMs, which simultaneously models both winding sets. A tool featuring the aforementioned capability might result useful for investigating the mutual thermal influence between the two winding sets, mainly when they work with different electric loads (i.e. asymmetric load operations). In other words, the temperature rise, occurring in one winding set and produced by the Joule losses within the other winding, could be evaluated. Conversely, a more accurate temperature estimation could be achieved, when only one winding set is supplied, whilst the second one is open (e.g. the winding set is open in response to a PEC failure) [4]. In this case, the 'complete' LPTN is able to account also for the part of heat generated inside the loaded slot and transferred to the unloaded one.

Considering all the above, the paper presents a thermal analysis of a dual three-phase PMSM, together with its 'complete' LPTN, where the thermal behaviour of both winding sets is addressed. The LPTN is experimentally fine-tuned LPTN using a custom-built PMSM prototype. The aim of the fine-tuning procedure consists in identifying the LPTN critical parameters, such as the slot equivalent thermal conductivity, the natural air convection coefficient, etc. [22]. By exploiting the geometric symmetry featured by the analysed PMSM, the nodes' number of the obtained LPTN is then minimized leading to a reduced order LPTN (i.e. 3-node), which still includes both winding sets. The elements of the new LPTN are easily determined and its performance is assessed against the measured temperature profiles, revealing a good fitting especially at steady-state. Finally, the computational effort of the two LPTNs (i.e. high- and low-order) is apprised and, as expected, a considerable simulation time reduction is observed when the reduced order LPTN is utilized.

This work was funded by the INNOVATIVE doctoral programme. The INNOVATIVE programme is partially funded by the Marie Curie Initial Training Networks (ITN) action (project number 665468) and partially by the Institute for Aerospace Technology (IAT) at the University of Nottingham.

This work was also partially funded by the University of Nottingham Propulsion Futures Beacon.

P. Giangrande, V. Madonna, S. Nuzzo C. Spagnolo, C. Gerada and M. Galea are all with the Power Electronics, Machines and Control (PEMC) group, University of Nottingham, Nottingham, NG72RD, UK (e-mail: p.giangrande@nottingham.ac.uk).

Chris Gerada and Michael Galea are also with the University of Nottingham Ningbo China, Ningbo 315100, China.

II. PMSM Description

The dual three-phase PMSM employed during the thermal investigation features a 12 slots / 10 poles combination and is equipped with a concentrated single-layer winding layout. The geometry and winding arrangement of the PMSM are shown in Fig. 1, while the main design parameters are listed in TABLE I. Both winding sets (i.e. set '1' and set '2') are star-connected and the shift angle between phase 'A1' and phase 'A2' axes is equal to zero degrees. The chosen winding topology complies with the fault-tolerance requirements [23], because high per-phase self-inductance and low (approximately zero) mutual inductance among phases are accomplished [3]. Additionally, the phase-to-phase short-circuit risk is reasonably mitigated, being the coils non-overlapped. The PMSM is naturally air cooled and an aluminium housing with axial fins is mounted for enhancing the heat transfer to the external ambient. For the sake of completeness, the housing engineering drawing is provided in Fig. 2.

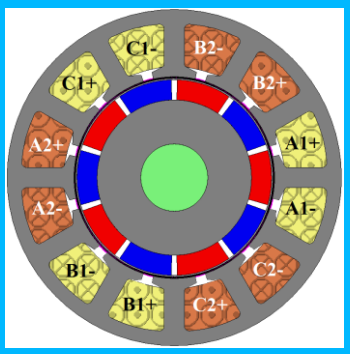

Fig. 1. Geometry and winding layout of the dual three-phase, 12 slots / 10 poles PMSM.

TABLE I. Dual Three-Phase PMSM Parameters

Parameter	Symbol	Value
Rated Speed [rpm]	Ω_{PMSM}	2500
Rated Torque [Nm]	τ_{PMSM}	1
Rated Current [A_{rms}]	I_n	2.2
Phase Resistance [Ω]	R	3.24
d- and q-axis Inductances [mH]	L_d and L_q	13.7
PM Flux [Wb]	Ψ_{PM}	0.112
Stack Length [mm]	L	50
Stator Outer Diameter [mm]	D_o	50

III. Complete High-Order LPTN

In general, LPTNs provide a precise temperature estimation with low computational time compared to computational fluid dynamics (CFDs) [11] or finite element (FE) methods [16]. Nevertheless, some LPTN parameters, also known as critical parameters [21], are not easy to be analytically calculated, due to the uncertainty of material properties, and they strongly influence the LPTN accuracy. Hence, the LPTN critical parameters are experimentally quantified for the PMSM at hand (i.e. LPTN fine-tuning procedure). The tests are performed by feeding both winding sets via as many independent DC power supplies. It is worth to point out that, by using DC sources, the thermal contribution of the PMSM iron losses is neglected, as well as, the impact of skin and proximity effects on the winding electrical resistance. This choice (i.e. DC tests) does not compromise their validity, because the relatively low PMSM fundamental frequency (i.e. ≈208 Hz), combined with the small wire cross-section adopted (i.e. AWG 26), makes reasonable the assumption of neglecting skin and proximity effects. Further, the FE simulation results prove that the main share to the PMSM losses is given by the Joule losses. Therefore, the iron losses only slight affect the hot-spot temperature, thus it is appropriate to exclude them from the thermal model.

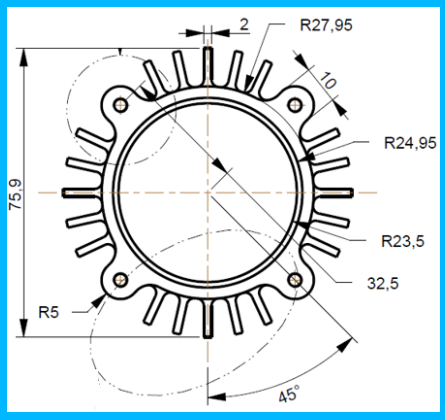

Fig. 2. Engineering drawing of the PMSM aluminum housing (all dimensions are in mm).

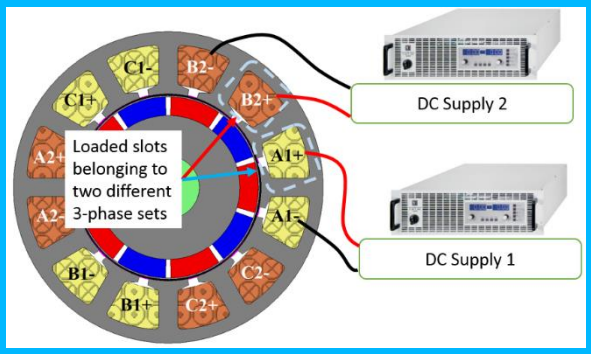

Fig. 3. DC power supplies layout employed during thermal tests.

The DC voltages are applied as depicted in Fig. 3, where two phases ('A1' and 'B2' in the figure), each belonging to different winding sets and hosted in adjacent slots, are simultaneously loaded. The described measurement layout permits to examine the mutual thermal influence between the two winding sets. The winding temperatures are measured by means of K-type thermocouples, which are uniformly distributed within the PMSM's windings, with the purpose of detecting the hot-spot temperature. The recorded temperatures are elaborated through an acquisition board connected to a personal computer. The whole thermal test setup is shown in Fig. 4, where the PMSM under test, both DC power supplies and the data logger are highlighted.

Knowing the materials and the geometric dimensions of the PMSM, the high-order LPTN is built, as illustrated in Fig. 5. The procedure for computing the thermal resistances and capacitances can be found in [15] and thus, it is not reported in this paper. The LPTN is developed under the assumption that no-heat transfer occurs along the axial direction, consequently only radial and circumferential resistances are modelled. In addition, the rotor is considered as thermally insulated from the ambient (i.e. no-heat transfer across shaft and bearings). This choice is justified by the convenience of having a conservative LPTN. With the aim of evaluating the thermal effect, due to different combinations of Joule losses

generated by the currents flowing throughout the two PMSM's stars, two slots are implemented in the LPTN, each belonging to one winding set. However, the presence of both slots inevitably increases the LPTN nodes and its computational burden. Finally, between stator and housing, a tiny air interface (i.e. t_{int} thickness) is incorporated in the LPTN. Hence, the stator core is thermally connected to the finned housing via an interference thermal resistance.

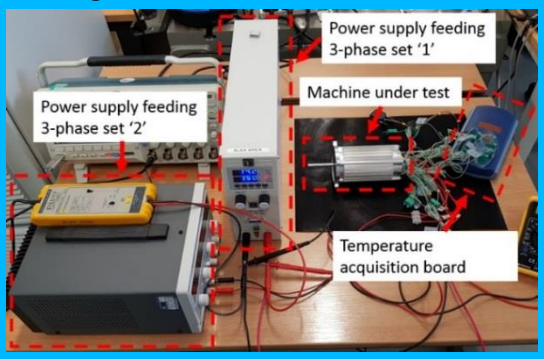

Fig. 4. Complete experimental setup for the thermal tests.

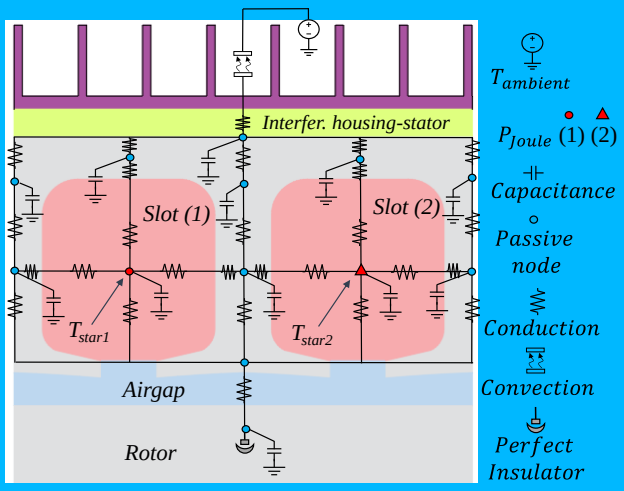

Fig. 5. PMSM high-order LPTN modelling two slots.

TABLE II. EXPERIMENTALLY-TUNED CRITICAL PARAMETERS

Parameter	Description	Value
h_{air} [$W/m^2/K$]	Air natural convection	5
k_{air} [$W/m/K$]	Air conductivity	0.0658
k_{slot} [$W/m/K$]	Equivalent slot conductivity	0.346
k_{iron} [$W/m/K$]	Iron conductivity	27.34
C_{hous} [J/K]	Housing capacitance	100
C_{tooth} [J/K]	Tooth capacitance	2.97
$C_{yoke\text{-}slot}$ [J/K]	Yoke capacitance (slot section)	1.57
$C_{yoke\text{-}tooth}$ [J/K]	Yoke capacitance (tooth section)	1.19
C_{slot} [J/K]	Slot capacitance	7.36
t_{int} [mm]	Int. housing-stator thickness	2.03e-2

Based on the outcomes of the thermal tests (i.e. experimental temperature profiles), the values of the critical parameters are estimated by means of the *Simulink® Design Optimization Toolbox*, allowing for the LPTN fine-tuning. In detail, for several DC current combinations (i.e. I_{star1} and I_{star2} pairs), the measured hot-spot temperature profiles of both winding sets (T_{star1} and T_{star2}) are imported and pre-processed by the toolbox, which determines the critical parameters using a sequential quadratic programming (SQP) algorithm [5]. The list of these parameters is given in TABLE II, alongside with their values. Once the high-order LPTN is fine-tuned, it is used for predicting the PMSM hot-spot temperatures of each winding set, for different combinations of currents flowing into the two three-phase windings.

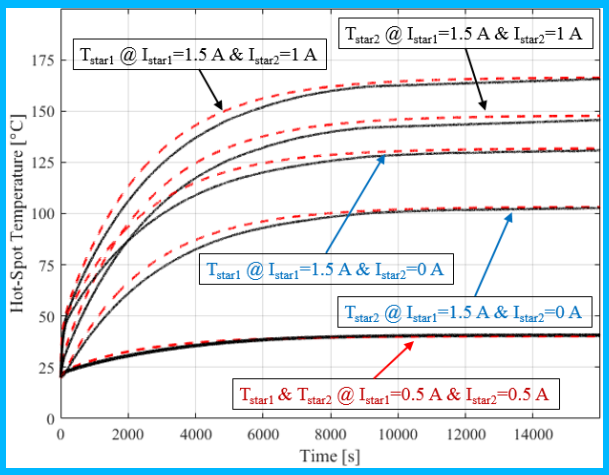

Fig. 6. Hot-spot temperature profiles for different load conditions: experimental (black continuous line) and LPTN-predicted (red dashed line).

In order to assess the effectiveness of the high-order thermal model, the LPTN-predicted temperature profiles are compared to those measured, for the following loading states: 1) one winding set loaded, while the other one is open (i.e. I_{star1}=1.5 A and I_{star2}=0 A), 2) both winding sets loaded, but at different current levels (i.e. I_{star1}=1.5 A and I_{star2}=1 A) and 3) the same current flows in the winding sets (i.e. I_{star1}=I_{star2}=0.5 A). The obtained results are shown in Fig. 6, which reveals an excellent match between measured and estimated temperatures, during steady-state and transient conditions. Analysing the temperature profiles corresponding to cases when I_{star1}=1.5 A (i.e. cases 1 and 2), it is evident the thermal coupling between the winding sets. In fact, if I_{star2}=0 A, the resulting T_{star1} is lower than the value that would be predicted by a LPTN modelling just one slot, as the heat from the loaded slot is actually transferred to the external ambient and the unloaded slot (i.e. slot 2). On the other hand, if I_{star2}=1 A, the ensuing T_{star1} is higher than the value estimated in the previous case (I_{star2}=0 A), due to a lower thermal gradient between the slots (i.e. smaller amount of heat produced in slot 1 and migrating towards slot 2).

Despite the good estimation performance of the high-order LPTN, its complex structure (i.e. elevate number of nodes) makes the thermal model inconvenient for real-time applications and/or fast temperature prediction. Besides the layout complexity, the significant number of critical parameters to be identified (i.e. 10) yields to a time-costly fine-tuning. These drawbacks led to the development of a low-order LPTN, which represents one of the main outcomes of this work. The low-order LPTN is discussed in the next section.

IV. LOW-ORDER LPTN

The tests campaign findings have confirmed that the PMSM hot-spot temperatures are located within the windings. Therefore, relying on the PMSM geometric symmetry, the LPTN presented in Fig. 5 is simplified, focusing on the slot with the purpose of deriving a reduced order LPTN. As depicted in Fig. 7, the new LPTN consists in only 3 thermal

resistances and 2 thermal capacitances, resulting in a total number of nodes equal to 3. The choice of a 3-node LPTN is supported by the interest of giving preference to the LPTN simplicity. In particular, two thermal resistances are employed for modelling the heat transfer from each slot to the external ambient, and due to the symmetric structure, they are characterized by the same numerical value (i.e. R_k). The third thermal resistance (i.e. R_j) connects the two slots and it accounts for the heat exchanged between them (i.e. thermal coupling). Finally, the two thermal capacitances (i.e. C_k) featuring identical values (based on the PMSM symmetry) are placed in every slot.

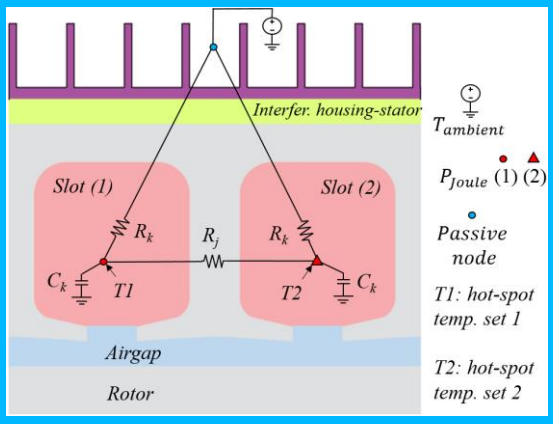

Fig. 7. PMSM low-order LPTN modelling two slots.

Having outlined the reduced LPTN layout characterized by only 3 nodes, the procedure for determining its components is presented. Considering the steady-state conditions, the thermal capacitances can be removed from the circuit of Fig. 7 and the thermal resistances R_k and R_j can be expressed according to (1) and (2), respectively.

$$R_K = \frac{T1+T2-2T_{ambient}}{P_{joule(1)}+P_{joule(2)}} \quad (1)$$

$$R_J = R_K \cdot \frac{T1-T2}{T2-T_{ambient}-R_K \cdot P_{joule(2)}} \quad (2)$$

where $T_{ambient}$ is the ambient temperature, T1 and T2 are the measured steady-state hot-spot temperatures of the corresponding slots, while $P_{joule(1)}$ and $P_{joule(2)}$ are the relative Joule losses. As a result of the experimental tests, all the above parameters are known quantities, hence, R_k and R_j are easily calculated. It is worthy to point out that (2) can be applied only when $I_{star1} \neq I_{star2}$. Further, only one experimental test, under asymmetric electric load condition (i.e. $I_{star1} \neq I_{star2}$), is required for defining R_k and R_j. Once these resistances are computed, the capacitance value C_k is identified following the same approach previously adopted for the critical parameters estimation (i.e. *Simulink® Design Optimization Toolbox*). Nevertheless, a much lower computational time is needed at this round, due to the restrained number of unknowns (i.e. only C_k). The reduced order LPTN parameters are listed in TABLE III, alongside with their numerical values. The prediction performance of the obtained low-order LPTN is evaluated in both symmetric ($I_{star1}=I_{star2}$) and asymmetric ($I_{star1} \neq I_{star2}$) electric load operations. In Fig. 8, both experimental and low-order LPTN-predicted temperature profiles are shown for 0.5 A and 1 A symmetric load conditions. For the sake of clarity, just the temperature profiles of slot 1 (i.e. T1) are reported in Fig. 8, since T1 and T2 profiles result overlapped. As expected, the reduced order LPTN is capable of estimating the steady-state temperature with a very good accuracy (i.e. error below 3%). On the other hand, the 3-node LPTN tends to overestimate the temperature during the transients, where the mismatch between measured and predicted temperatures increases. This discrepancy can be ascribed to the implementation of only two capacitances in the reduced order LPTN. Regarding the asymmetric electric load operations, the following current combinations are considered: 1) I_{star1}=1.5 A and I_{star2}=1 A plus 2) I_{star1}=1A and I_{star2}=0.5 A. The comparison outcome is summarized in Fig. 9, where as in the previous case, an excellent precision is achieved at steady-state, whilst a higher estimation error is observed when the temperature rises.

TABLE III. PARAMETERS OF THE LOW-ORDER LPTN

Parameter	Value
R_k [K/W]	45.9
R_j [K/W]	19.5
C_k [J/K]	44.6

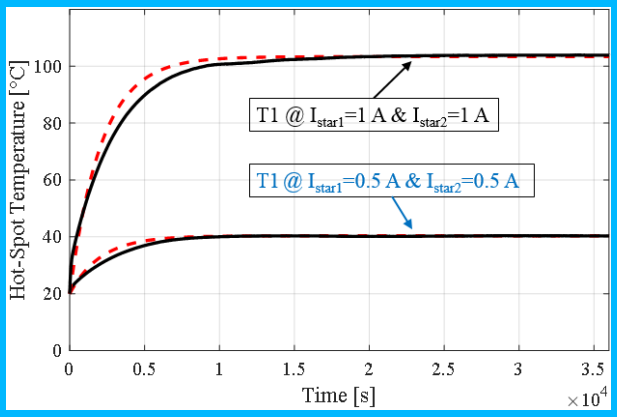

Fig. 8. Hot-spot temperatures in symmetric load conditions: experimental (black continuous) and low-order LPTN-predicted (red dashed) profiles.

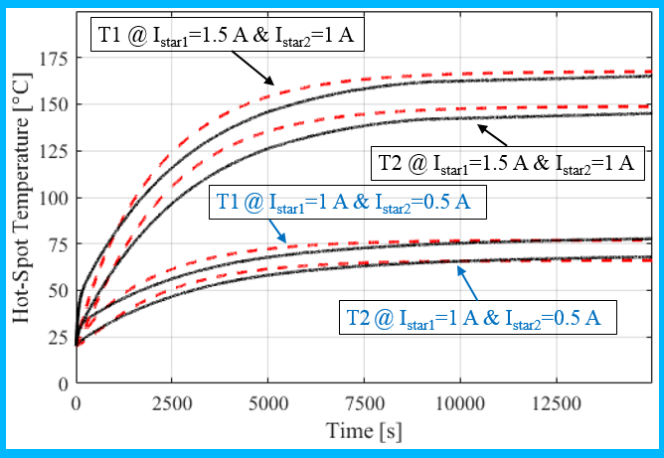

Fig. 9. Hot-spot temperatures in asymmetric load conditions: experimental (black continuous) and low-order LPTN-predicted (red dashed) profiles.

V. LPTNs PERFORMANCE COMPARISON

In this section, the two presented LPTNs (i.e. high- and low-order) are evaluated in terms of accuracy and computational effort. Assuming PMSM symmetric load

operations, the hot-spot LPTN-predicted temperature profiles are plotted alongside with the measured values. In Fig. 10, their comparison is shown considering only T1 (for the sake of figure clarity), while the temperature estimation errors, calculated against the experimental temperature, are reported in Fig. 11, for I_{star1}=I_{star2}=1.4 A (top subplot) and I_{star1}=I_{star2}=1 A (bottom subplot). For highlighting the transient mismatch, a logarithmic time-scale is used in Fig. 11.

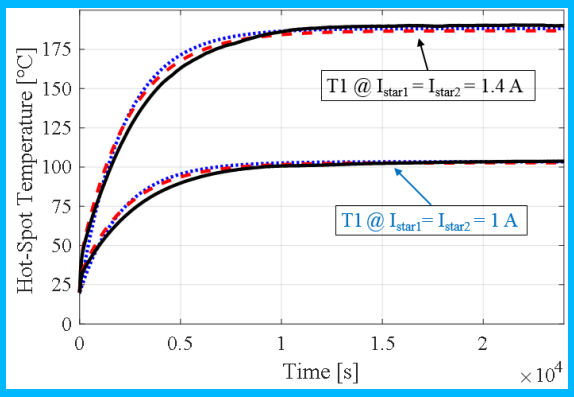

Fig. 10. Hot-spot temperatures in symmetric load conditions: measured (black continuous), high-order LPTN-predicted (red dashed) and low-order LPTN-predicted (blue dotted).

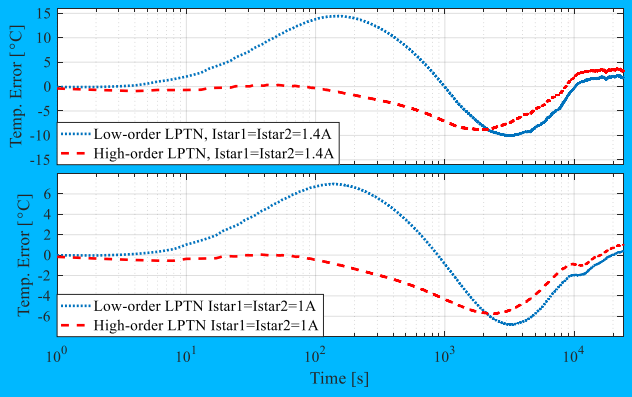

Fig. 11. Temperature prediction errors for I_{star1}=I_{star2}=1.4 A (top subplot) and I_{star1}=I_{star2}=1 A (bottom subplot).

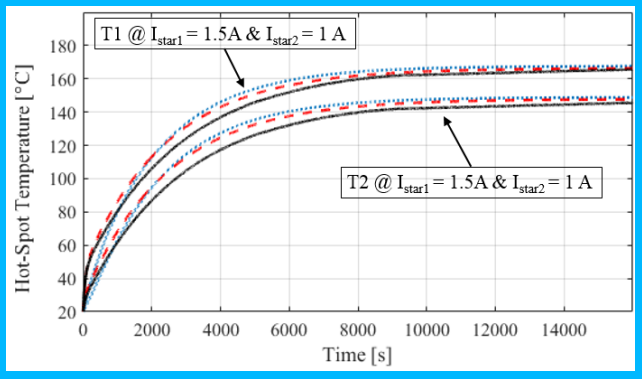

Fig. 12. Hot-spot temperatures in asymmetric load conditions: measured (black continuous), high-order LPTN-predicted (red dashed) and low-order LPTN-predicted (blue dotted).

This analysis confirms that during the temperature rise, the low-order LPTN reveals a greater estimation error with respect to the high-order one. In particular, the maximum mismatch is observed in the time-window from 50 s to 400 s. In transient conditions, as previously mentioned, the poor accuracy of the reduced order LPTN is mainly due to the small number of capacitances employed. Such drawback represents the price to pay for a fast and easy-to-tune LPTN.

For completeness, the LPTNs estimation capability is also tested in asymmetric electric load operations, namely I_{star1}=1.5 A and I_{star2}=1 A. As depicted in Fig. 12, the LPTN-predicted temperature profiles (T1 and T2) are compared between them and versus the experimental outcomes, whilst the corresponding estimation errors are given in Fig. 13, for both slot 1 (top subplot) and slot 2 (bottom subplot). Considerations similar to those carried out for Fig. 11 can be extended to the results of Fig. 13.

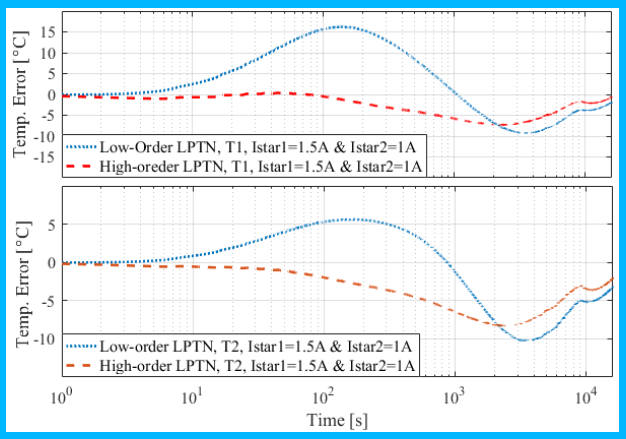

Fig. 13. Slot 1(top subplot) and slot 2 (bottom subplot) temperature prediction errors when I_{star1}=1.5 A and I_{star2}=1 A.

Finally, the LPTNs computational effort is investigated by implementing the LPTNs in Simulink® Simscape® environment and recording their simulation times. For this study, a personal computer equipped with an Intel® Xeon® E5-1620 3.50 GHz processor and 32*GB* of RAM is utilized. In order to guarantee for a fair comparison, identical simulation period (i.e. 20000 s) and solver are adopted. For performing a full-transient simulation, the high-order LPTN takes 28.12 s, whereas 3.44 s are required by the low-order LPTN. According to these findings, it can be concluded that the high-order LPTN is more suitable than the low-order one for a thermal analysis at the design stage of the dual three-phase PMSM, due to its higher accuracy. However, a motorette resembling the designed PMSM should be employed for the fine-tuning of the critical parameters. On the contrary, the reduced order LPTN is advisable for on-line temperature estimation seeing its low computational burden.

VI. Conclusions

In this paper, the detailed thermal analysis of a dual three-phase PMSM was carried out, by developing two LPTNs with different levels of complexity. Aiming at modelling the thermal coupling between the two winding sets, these LPTNs have the peculiarity of including two slots (each belonging to a distinct winding set), which allows to predict the hot-spot temperatures under symmetric and asymmetric load conditions of the considered platform.

First, a high-order LPTN was developed and its performance was evaluated via experimental results. The high-order LPTN provides very accurate results at the cost of a significant computational time and a complex fine-tuning procedure for determining the LPTN critical parameters. Due to these drawbacks, a 3-node LPTN was then built exploiting

the inherent PMSM geometric symmetry. In favour of the computational speed, the simplest possible LPTN was preferred to medium complexity architectures. The procedure for calculating the reduced order LPTN's components was described and its simplicity was highlighted. Only a single experimental test, in asymmetric load conditions, is needed for identifying the relevant thermal resistances. Although poor estimation accuracy during transient was registered due to the reduced number of thermal capacitances adopted, the low-order LPTN has shown outstanding potential for fast estimation of the PMSM's thermal behaviour. Further investigations are in place for improving the low-order LPTN prediction performance throughout the temperature rise, while keeping its complexity moderate.

VII. REFERENCES

[1] W. Cao, B.C. Mecrow, G.J. Atkinson, *et al.*, "Overview of Electric Motor Technologies Used for More Electric Aircraft (MEA)," *IEEE Transactions on Industrial Electronics*, vol. 59, pp. 3523-3531, 2012.

[2] P. Giangrande, V. Madonna, S. Nuzzo and M. Galea, "Design of Fault-Tolerant Dual Three-Phase Winding PMSM for Helicopter Landing Gear EMA," *in 5th International Conference on Electric Systems for Aircraft, Ship Propulsion and Road Vehicles (ESARS)*, 2018.

[3] V. Madonna, P. Giangrande, C. Gerada, and M. Galea, "Thermal analysis of fault-tolerant electrical machines for aerospace actuators," *in press on IET Electric Power Applications*, DOI: 10.1049/iet-epa.2018.5153, 2018.

[4] M. Barcaro, N. Bianchi, and F. Magnussen, "Faulty Operations of a PM Fractional-Slot Machine With a Dual Three-Phase Winding," *IEEE Transactions on Industrial Electronics*, vol. 58, pp. 3825-3832, 2011.

[5] C. Sciascera, P. Giangrande, C. Brunson, M. Galea, and C. Gerada, "Optimal design of an electro-mechanical actuator for aerospace application," *in IECON 2015 - 41st Annual Conference of the IEEE Industrial Electronics Society*, pp. 1903-1908, 2015.

[6] M. Barcaro, N. Bianchi, and F. Magnussen, "Analysis and Tests of a Dual Three-Phase 12-Slot 10-Pole Permanent-Magnet Motor," *IEEE Transactions on Industry Applications*, vol. 46, pp. 2355-2362, 2010.

[7] D. Casadei, F. Filippetti, M. Mengoni, *et al.*, "Detection of magnet demagnetization in five-phase surface-mounted permanent magnet generators," *in 3rd IEEE International Symposium on Power Electronics for Distributed Generation Systems* (PEDG), 2012.

[8] D. Casadei, M. Mengoni, G. Serra, *et al.*, "Optimal fault-tolerant control strategy for multi-phase motor drives under an open circuit phase fault condition," *in 18th International Conference on Electrical Machines (ICEM)*, 2008.

[9] J. Pyrhonen, T. Jokinen, and V. Hrabovcova, *Design of rotating electrical machines*: John Wiley & Sons, 2009.

[10] A. Al-Timimy, M. Degano, Z. Xu, G. Lo Calzo, P. Giangrande, M. Galea, C. Gerada, H. Zhang and L. Xia, "Trade-off analysis and design of a high power density PM machine for flooded industrial pump," *in 42nd Annual Conference of the IEEE Industrial Electronics Society (IECON)*, 2016.

[11] K. Bersch, S. Nuzzo, P. Giangrande, A. Walker, and M. Galea, "Combined Thermofluid and Electromagnetic Optimization of Stator Vent Cooling," *in XIII International Conference on Electrical Machines (ICEM)*, 2018.

[12] A. Al-Timimy, M. Degano, P. Giangrande, G.L. Calzo, Z. Xu, M. Galea, C. Gerada, H. Zhang and L. Xia, "Design and optimization of a high power density machine for flooded industrial pump," in *22nd International Conference on Electrical Machines (ICEM)*, 2016.

[13] V. Madonna, P. Giangrande, and M. Galea, "Electrical Power Generation in Aircraft: review, challenges and opportunities," in *IEEE Trans. on Transportation Electrification*, vol. 4, pp. 646 - 6591, 2018.

[14] V. Madonna, A. Walker, P. Giangrande, C. Gerada, G. Serra, and M. Galea, "Improved thermal management and analysis for stator end-windings of electrical machines," *in press on IEEE Transactions on Industrial Electronics*, DOI: 10.1109/TIE.2018.2868288, 2018.

[15] V. Madonna, P. Giangrande, A. Walker, and M. Galea, "On the Effects of Advanced End-Winding Cooling on the Design and Performance of Electrical Machines," *in XIII International Conference on Electrical Machines (ICEM)*, 2018.

[16] A. Boglietti, D. Cavagnino, M. Staton, *et al.*, "Evolution and modern approaches for thermal analysis of electrical machines," in *IEEE Trans. on Industrial Electronics*, vol. 56, no. 3, pp. 871–882, 2009.

[17] Z. Xu, A. Al-Timimy,M. Degano, P. Giangrande, G. Lo Calzo, H. Zhang, M. Galea, C. Gerada, S. Pickering, and L. Xia, "Thermal management of a permanent magnet motor for a directly coupled pump," in *International Conference on Electrical Machines (ICEM)*, 2016.

[18] T. W. Dakin, "Electrical Insulation Deterioration Treated as a Chemical Rate Phenomenon," in *Transactions of the American Institute of Electrical Engineers*, vol. 67, pp. 113-122, 1948.

[19] G. C. Montanari and L. Simoni, "Aging phenomenology and modeling," in *IEEE Transactions on Electrical Insulation*, vol. 28, pp. 755-776, 1993.

[20] P. Lindh, M.G. Tehrani, T. Lindh, J.H. Montonen, *et al.*, "Multi-disciplinary Design of a Permanent-Magnet Traction Motor for a Hybrid Bus Taking the Load Cycle into Account," in IEEE Trans. Ind. Electron., vol. 63, pp. 3397-3408, 2016.

[21] B. Vaseghi, N. Takorabet, J.P. Caron, *et al.*, "Study of Different Architectures of Fault-Tolerant Actuator Using a Two-Channel PM Motor," in *Trans. on Industry Applications*, vol. 47, pp. 47-54, 2011.

[22] A. Boglietti, A. Cavagnino, and D. Staton, "Determination of Critical Parameters in Electrical Machine Thermal Models," in *IEEE Transactions on Industry Applications*, vol. 44, pp. 1150-1159, 2008.

[23] B.A. Welchko, T.A. Lipo, T.M. Jahns, *et al.*, "Fault tolerant three-phase AC motor drive topologies: a comparison of features, cost, and limitations," in *IEEE Trans. on Power Electronics*, vol. 19, 2004.

VIII. BIOGRAPHIES

Paolo Giangrande received his PhD in electrical engineering at the Politecnico of Bari in 2011. Since January 2012, he is Research Fellow at the University of Nottingham (UK), within the Power Electronics, Machines and Control (PEMC) group. His main research interests include design and testing of electromechanical actuators for aerospace, thermal management of high-performance electric drives and reliability of electrical machines.

Vincenzo Madonna received the BSc degree in Electronic Engineering from University of Calabria, Italy, in 2012 and the MSc degree in Electrical Engineering from the University of Bologna, Italy, in 2016. He is currently a Marie Curie Fellow and PhD candidate in electrical machines design within the Institute for Aerospace Technology (IAT) and the PEMC group at the University of Nottingham, UK. His research interests include design, thermal management and lifetime prediction modelling of electrical machines.

Stefano Nuzzo received the Ph.D. degree in Electrical Machine Design in 2018 from the University of Nottingham, Nottingham, U.K, where he is currently working as a Research Fellow within the PEMC Group. His current research interests are the analysis, modelling and optimizations of electrical machines, with focus on salient-pole synchronous generators and brushless excitation systems for industrial power generation applications.

Cosimo Spagnolo received his B.Sc. degree in Electronic Engineering from the University of Messina, Messina, Italy, in 2013 and M.Sc. degree in Electrical Engineering from the University of Bologna, Bologna, Italy, in 2016. He is currently a Ph.D. student and Marie-Curie Early Stage Researcher at the Institute for Aerospace Technology Center at the University of Nottingham and also member of PEMC. His current research interests include the analytical approach to design of electrical distribution systems for aircraft.

Chris Gerada received the Ph.D. degree in numerical modelling of electrical machines from University of Nottingham (U.K), in 2005. He subsequently worked as a researcher with University of Nottingham on high-performance electrical drives and on the design and modelling of electromagnetic actuators for aerospace applications. In 2013, he was appointed as a Professor at University of Nottingham. He serves as an associate editor for the IEEE transaction on industry applications. His main research interests include the design and modelling of electric drives and machines.

Michael Galea received his PhD in electrical machines design from the University of Nottingham, where he has also worked as a Research Fellow. He is currently the Head of the School of Aerospace in the University of Nottingham, Ningbo, China. His main research interests are design, analysis and thermal management of electrical machines and drives, the more electric aircraft and electrified and hybrid propulsion.